A Navier-Stokes Nozzle Analysis Technique

Jeffrey J. Brown*
Boeing Commercial Airplane Company, Seattle, Washington

A method for calculating the flowfield in propulsive nozzles is presented. The complete set of partial differential equations for time-dependent, compressible, viscous flow are solved using an efficient numerical procedure. The flowfield is subdivided into rectangular regions called cells and the fluxes of conserved properties (mass, momentum, and energy) into each cell are balanced using a finite-volume approach. Solid boundary conditions are enforced using an imaginary row of cells inside the body, while inflow and outflow boundary conditions are enforced using a method of characteristics formulation. The line Gauss-Seidel implicit technique of MacCormack is used to solve the Reynolds-averaged Navier-Stokes equations in the computational domain. The Baldwin-Lomax algebraic turbulence model is used. Multistream, axisymmetric nozzle flowfields, including mixing of the streams, can be analyzed using this method. A fan nozzle thrust reverser can be analyzed as well. Results are presented for a converging-diverging propulsive nozzle, multistream turbofan nozzles, and a turbofan nozzle with a thrust reverser. The computational results show excellent agreement with the experimental data. A two order of magnitude reduction in run cost relative to the MacCormack explicit method is demonstrated.

Nomenclature

a = speed of sound
A = axial Jacobian matrix or flow area
A = area of a cell face times the unit vector normal to that face
B = radial Jacobian matrix
c_v = specific heat at constant volume
D = difference operator
e = total energy per unit volume
F = axial flux vector
F = force vector
G = radial flux vector
I = identity matrix
k = thermal conductivity
M_y = matrix containing the implicit viscous terms
n = direction normal to a boundary
N = matrix translating conservative form to nonconservative form
P = pressure
$\dot{Q}$ = rate of heat transfer into a control volume
R = gas constant
t = time
T = temperature
u = axial component of velocity
U = vector containing the conservative variables
v = radial component of velocity
V = velocity magnitude
V = velocity vector
$\dot{W}$ = rate of work done on a control volume
x = axial coordinate
y = radial coordinate
α = specific kinetic energy
β = term in the Jacobian matrices, $\beta = \gamma - 1$
γ = ratio of specific heats
δU = change in the conservative variables
Δt = time step size
ΔU = physical change in the conservative variables
Δx = axial step size
Δy = radial step size
ϵ = specific internal energy
λ = second coefficient of viscosity
μ = first coefficient of viscosity
ρ = density
ρu = axial component of momentum per unit volume
ρv = radial component of momentum per unit volume
σ = normal stress
τ = shear stress

Superscripts

n = current time level
$n+1$ = next time level

Subscripts

B = value at boundary
i = axial index
j = radial index
$+$ = forward difference
$-$ = backward difference

Received May 27, 1986; presented as Paper 86-1613 at the AIAA/ASME/SAE/ASEE 22nd Joint Propulsion Conference, Huntsville, AL, June 16–18 1986; revision received Oct. 23, 1986.

*Senior Specialist Engineer, Nacelle Aerodynamics Group, Propulsion Research Unit.

Introduction

THE compressible form of the Reynolds-averaged Navier-Stokes equations adequately describes aerodynamic flow at the the temperatures and pressures encountered by commercial aircraft. If these equations could be efficiently solved, they would provide a very useful tool to augment wind-tunnel testing in the design of aircraft components. Much progress has been made toward the numerical solution of flowfields past complete aircraft configurations at flight Reynolds numbers. Even so, it is beyond present capabilities to perform these calculations in a design environment (wherein many configurations must be tested in order to determine the optimum design).

The progress made in the solution of the full potential and Euler equations (simplified versions of the Navier-Stokes equations) is great. The pioneering work of Murman and Cole[1] gave a simple, straightforward technique for solving the small-disturbance potential equations. Reyhner[2] has developed a three-dimensional full potential analysis based upon Murman and Cole's work, which provides good results

for weak shocks and attached boundary layers. When coupled with McLean's three-dimensional boundary-layer analysis,[3] Reyhner's code has been used successfully to predict the angle of attack at which an engine inlet will separate. This system will not yield information about whether a lip separation will reattach, however. Jameson et al.[4] Euler analysis methods have been applied to three-dimensional aircraft configurations with good results.[5] Flows with attached boundary layers can also be analyzed with an Euler analysis coupled to a boundary-layer code.

However, for flow complications such as turbulent separated flow, turbulent mixing processes, or shock boundary-layer interactions, the solution of the Reynolds-averaged Navier-Stokes equations with turbulence modeling is required. The calculation of the flowfield in a high-bypass-ratio turbofan nozzle requires a viscous formulation of the problem. An application of one economical Navier-Stokes solution technique to an axisymmetric nozzle flowfield is discussed in this paper.

Most common Navier-Stokes algorithms employ a time-dependent marching procedure. An initial guess at the solution is provided and the procedure "marches" in time to the steady state corresponding to the boundary conditions. This technique is used to circumvent the numerical complexities involved with flow in the transonic regime. A time-dependent solution is hyperbolic in time for all flow regimes. Consequently, one numerical procedure can be used throughout the flowfield. A steady formulation changes character from subsonic to supersonic flow (hence, different numerical techniques must be employed in each regime).

An explicit numerical procedure is the most straightforward to program. Unfortunately, the size of the time step in an explicit, time-dependent procedure is limited by stability considerations. The allowable time step size is proportional to the mesh spacing. Hence, when a very fine mesh is used to resolve the details of a flowfield (e.g., boundary layers or shock waves), the allowable time step size is also very small. Perry and Forester[6] and Cline and Wilmoth[7] employed the MacCormack explicit technique[8] to calculate multistream nozzle flowfields with good accuracy. Those schemes have proved to be too expensive to employ in a design environment due to the explicit time step size limitation.

Recent work on implicit algorithms has provided promising results.[9-11] An implicit time-dependent formulation has no stability limitation on the size of the time step. Theoretically, an implicit formulation could reach the steady-state limit much faster (hence less expensively) than an explicit analysis. MacCormack has developed a line Gauss-Seidel procedure[11] that reduces to Newton's method for very large time step sizes. That procedure yields economical solutions to nozzle flowfields. Some results from a nozzle flowfield analysis code, based upon MacCormack's implicit technique, are reported in this paper.

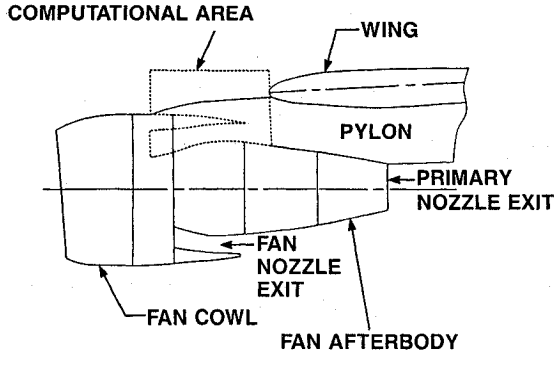

a) Geometry.

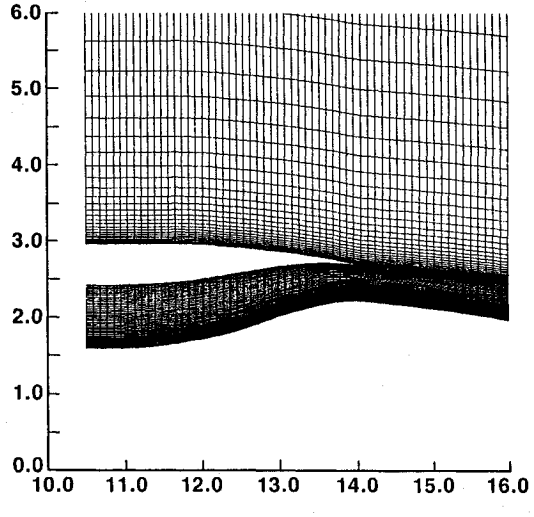

b) Computational area.

Fig. 1 Typical finite volume grid.

Numerical Algorithm

The set of equations which describes the physics of compressible, viscous flow are the time-dependent, Reynolds-averaged, Navier-Stokes equations. The Navier-Stokes equations, in two-dimensional conservative form, can be written as

$$\frac{\partial U}{\partial t}+\frac{\partial F}{\partial x}+\frac{\partial G}{\partial y}=0 \tag{1}$$

where

$$U=\begin{Bmatrix}\rho\\ \rho u\\ \rho v\\ e\end{Bmatrix},\quad F=\begin{Bmatrix}\rho u\\ \rho u^2+\sigma_x\\ \rho uv+\tau_{xy}\\ (e+\sigma_x)u+\tau_{yx}v-k\dfrac{\partial T}{\partial x}\end{Bmatrix}$$

$$G=\begin{Bmatrix}\rho v\\ \rho uv+\tau_{yx}\\ \rho v^2+\sigma_y\\ (e+\sigma_y)v+\tau_{xy}u-k\dfrac{\partial T}{\partial y}\end{Bmatrix}$$

$$\sigma_x=P-\lambda\left(\frac{\partial u}{\partial x}+\frac{\partial v}{\partial y}\right)-2\mu\frac{\partial u}{\partial x}$$

$$\tau_{xy}=\tau_{yx}=-\mu\left(\frac{\partial u}{\partial y}+\frac{\partial v}{\partial x}\right)$$

$$\sigma_y=P-\lambda\left(\frac{\partial u}{\partial x}+\frac{\partial v}{\partial y}\right)-2\mu\frac{\partial v}{\partial y}$$

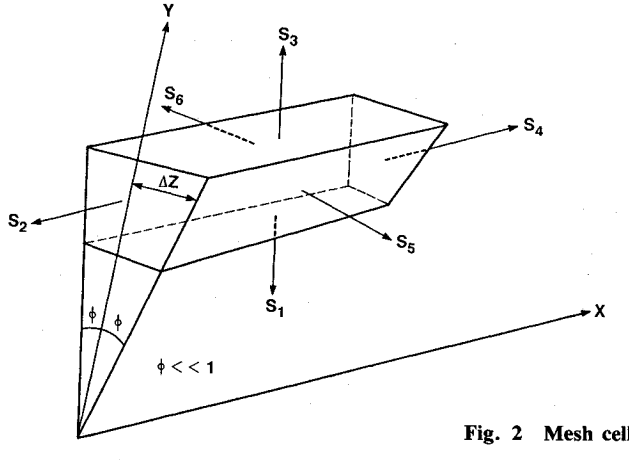

Fig. 2 Mesh cell.

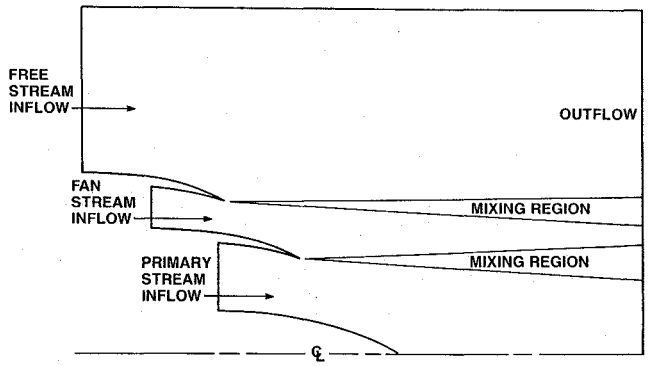

Fig. 3 Typical turbofan flowfield.

In terms of density ρ, axial and vertical velocity components u and v, respectively, total energy per unit volume e, temperature T, normal stress σ, shear stress τ, viscosity coefficients μ and λ, and thermal conductivity coefficient k. Finally, the pressure P is related to the specific internal energy ϵ and density ρ by an equation of state,

$$P=P(\rho,\epsilon) \tag{2}$$

The total energy per unit volume is comprised of the internal energy and the kinetic energy and is defined as

$$e=\rho\left(\epsilon+\frac{u^2+v^2}{2}\right)$$

This analysis assumes that the working fluid is a thermally and calorically perfect gas, thus,

$$P=\rho RT=\rho(\gamma-1)\epsilon \tag{3}$$

where γ is the ratio of specific heats.

The first coefficient of viscosity μ is calculated as a function of temperature using either the Sutherland law or a power law. The second coefficient λ is then obtained from Stokes' hypothesis as a constant (typically $-2/3$) times μ. The thermal conductivity k is calculated from the Prandtl number of the fluid. Turbulent flow effects are included in the physics by using the Baldwin-Lomax algebraic turbulence model.[12]

Finite-Volume Method

The finite-volume method is used in this analysis. Consider the integral form of the equations of motion,

$$\frac{\partial}{\partial t}\iiint \rho \mathrm{d}\mathcal{V}+\iint \rho \boldsymbol{V}\cdot\mathrm{d}\boldsymbol{A}=0 \tag{4}$$

$$\frac{\partial}{\partial t}\iiint \boldsymbol{V}\rho \mathrm{d}\mathcal{V}+\iint \boldsymbol{V}\rho \boldsymbol{V}\cdot\mathrm{d}\boldsymbol{A}=\boldsymbol{F}_S+\boldsymbol{F}_B \tag{5}$$

$$\frac{\partial}{\partial t}\iiint e\mathrm{d}\mathcal{V}+\iint\left(\epsilon+\frac{P}{\rho}+\frac{V^2}{2}\right)\rho \boldsymbol{V}\cdot\mathrm{d}\boldsymbol{A}=\dot{Q}+\dot{W} \tag{6}$$

Equations (4–6) describe the change in the mass ρ, momentum vector $\rho\boldsymbol{V}$, and total energy e (all per unit volume) within a control volume as a result of shear forces $\boldsymbol{F}_S$ and body forces $\boldsymbol{F}_B$ acting on the control volume, the rate of heat transfer into the control volume $\dot{Q}$, and the rate of work done on the control volume $\dot{W}$.

The flowfield is divided up into quadrilateral control volumes (Fig. 1) and Eqs. (4–6) are applied over each finite-control volume to calculate the solution. By assuming that the fluid properties are constant in each control volume and that each volume is constant in time, Eqs. (4–6) can be rewritten as

$$\frac{\partial\rho}{\partial t}=-\frac{\rho}{\mathcal{V}}\iint \boldsymbol{V}\cdot\mathrm{d}\boldsymbol{A} \tag{7}$$

$$\frac{\partial\rho\boldsymbol{V}}{\partial t}=\frac{1}{\mathcal{V}}\left(\boldsymbol{F}_S+\boldsymbol{F}_B-\rho\boldsymbol{V}\iint \boldsymbol{V}\cdot\mathrm{d}\boldsymbol{A}\right) \tag{8}$$

$$\frac{\partial e}{\partial t}=\frac{1}{\mathcal{V}}\left(\dot{Q}+\dot{W}-(e+P)\iint \boldsymbol{V}\cdot\mathrm{d}\boldsymbol{A}\right) \tag{9}$$

where

$$e=\rho\left(\epsilon+\frac{V^2}{2}\right)$$

Rewriting Eq. (1), one obtains

$$\frac{\partial U}{\partial t}=\frac{\partial}{\partial t}\begin{Bmatrix}\rho\\ \rho u\\ \rho v\\ e\end{Bmatrix}=-\frac{\partial F}{\partial x}-\frac{\partial G}{\partial y}=\Delta U \tag{10}$$

The right-hand sides of Eqs (7–9) represent a means to calculate ΔU, the flux of the fluid properties into each finite-volume cell.

Axisymmetric solutions are obtained using the Cartesian coordinate form of the governing equations (1) with the following modifications. The cell depth is made proportional to the Cartesian coordinate y, as shown in Fig. 2. An additional normal stress, which acts upon cell surfaces 5 and 6 shown in Fig. 2, is included in the set of difference equations. Shear stresses acting on surfaces 5 and 6 are estimated to be small in comparison to the normal stresses and are therefore neglected. Since the angle shown in Fig. 2 is made arbitrarily small, axisymmetric solutions result. Hence, y corresponds to the radial coordinate and v to the radial velocity component.

Flux-Vector Splitting

There are certain flow conditions, such as shock waves or other high-gradient regions of the flowfield, where the straightforward determination of the cellular fluxes is not accurate enough. Steger and Warming[13] developed a technique called flux-vector splitting to calculate the cellular fluxes taking into account the physical directions of the information propagation within the fluid. This yields a very accurate representation of the cellular fluxes and is used in this analysis when needed.

The flux terms F and G can be split into inviscid and viscous parts. This is illustrated by the following for F:

$$F=F'_{\substack{\text{inviscid}\\ \text{part}}}+F''_{\substack{\text{viscous}\\ \text{part}}} \tag{11}$$

The Jacobian of the inviscid part of the flux vector F with respect to U for a perfect gas is represented by

$$A=\frac{\partial F'}{\partial U} \tag{12}$$

Steger and Warming[13] point out that F' is homogeneous of degree one in the elements of U. This means that one can write

$$F'=AU \tag{13}$$

The Jacobian matrix A can be diagonalized by a similarity transformation S_x as follows:

$$A = S_x^{-1} \begin{bmatrix} u & 0 & 0 & 0 \\ 0 & u+a & 0 & 0 \\ 0 & 0 & u & 0 \\ 0 & 0 & 0 & u-a \end{bmatrix} S_x \tag{14}$$

where

$$S_x = \begin{bmatrix} 1 & 0 & 0 & -\frac{1}{a^2} \\ 0 & \rho a & 0 & 1 \\ 0 & 0 & 1 & 0 \\ 0 & -\rho a & 0 & 1 \end{bmatrix} \begin{bmatrix} 1 & 0 & 0 & 0 \\ -\frac{u}{\rho} & \frac{1}{\rho} & 0 & 0 \\ -\frac{v}{\rho} & 0 & \frac{1}{\rho} & 0 \\ \alpha\beta & -u\beta & -v\beta & \beta \end{bmatrix}$$

In general, some of the elements of this diagonalized matrix are positive and some negative. Their signs determine the direction of information travel. Let L^+ and L^- be two diagonal matrices containing, respectively, the positive and negative elements of the diagonalized matrix in Eq. (14). Then, the following two matrices can be defined:

$$A_+ = S_x^{-1} L^+ S_x \tag{15}$$

$$A_- = S_x^{-1} L^- S_x \tag{16}$$

The flux crossing the surface between the cell at (i, j) and the cell at $(i+1, j)$ is given by

$$F'_{i+\frac{1}{2},j} = A_+ U_{i,j} + A_- U_{i+1,j} \tag{17}$$

The first term on the right-hand side of Eq. (17) represents the contribution to the flux at surface $(i+\frac{1}{2},j)$ that travels to the right from cell (i,j), while the second term is the flux that travels to the left from cell $(i+1,j)$. Equation (17) represents a physically correct means of calculating the flux of the fluid properties into a cell and is used in the present analysis.

MacCormack Implicit Technique

To derive the implicit technique, one first differentiates the inviscid part of Eq. (1) with respect to time to obtain

$$\frac{\partial}{\partial t}\left(\frac{\partial U}{\partial t} + \frac{\partial F'}{\partial x} + \frac{\partial G'}{\partial y}\right) = 0$$

Substituting for the spatial difference operators, rearranging and substituting for the time derivative at time step n from Eq. (1), and defining

$$\Delta U^n = -\Delta t\left(\frac{DF^n}{\Delta x} + \frac{DG^n}{\Delta y}\right)$$

$$\delta U^{n+1} = \Delta t\left(\frac{\partial U}{\partial t}\right)^{n+1}$$

one obtains the implicit algorithm

$$\left(I + \Delta t\frac{D\cdot A}{\Delta x} + \Delta t\frac{D\cdot B}{\Delta y}\right)\delta U^{n+1} = \Delta U^n \tag{18}$$

where

$$A = \frac{\partial F'}{\partial U} \quad \text{and} \quad B = \frac{\partial G'}{\partial U}$$

are the Jacobian matrices of F' and G' with respect to U, respectively. In Eq. (18), the spatial difference operator D can be forward, backward, or central.

Viscous Terms

The matrices A and B are the Jacobians of the flux vectors F' and G', respectively. These vectors are the inviscid parts of the flux vectors F and G, respectively. The significant viscous terms appear in G (thin-layer Navier-Stokes equation) and are

$$G'' = -\begin{Bmatrix} 0 \\ \mu\frac{\partial u}{\partial y} \\ (\lambda+2\mu)\frac{\partial v}{\partial y} \\ u\mu\frac{\partial u}{\partial y} + v(\lambda+2\mu)\frac{\partial v}{\partial y} + k'\frac{\partial \epsilon}{\partial y} \end{Bmatrix} \tag{19}$$

where $k' = k/c_v$. The terms in G'' are approximated in the right-hand side of Eq. (18). Consequently, they must be balanced on the left-hand side by adding the following implicit term:

$$\left(I + \Delta t\frac{D\cdot A}{\Delta x} + \Delta t\frac{D\cdot B}{\Delta y} - \Delta t\frac{D\cdot M_y (D\cdot N/\Delta y)}{\Delta y}\right)\delta U^{n+1} = \Delta u^n \tag{20}$$

where

$$M_y = \begin{bmatrix} 0 & 0 & 0 & 0 \\ 0 & \mu & 0 & 0 \\ 0 & 0 & \lambda+2\mu & 0 \\ 0 & u\mu & v(\lambda+2\mu) & k' \end{bmatrix}, \quad \delta u = \begin{Bmatrix} \delta(\rho) \\ \delta(u) \\ \delta(v) \\ \delta(\epsilon) \end{Bmatrix}$$

But $\delta u = N\delta U$, where

$$N = \begin{bmatrix} 1 & 0 & 0 & 0 \\ \frac{-u}{\rho} & \frac{1}{\rho} & 0 & 0 \\ \frac{-v}{\rho} & 0 & \frac{1}{\rho} & 0 \\ \frac{\alpha-\epsilon}{\rho} & \frac{-u}{\rho} & \frac{-v}{\rho} & \frac{1}{\rho} \end{bmatrix}$$

Equation (18) is solved using line Gauss-Seidel relaxation. In the present implementation, two Gauss-Seidel relaxation sweeps are used for each time step. It can be shown that, as Δt becomes very large, Eq. (18) reduces to Newton's method for a system of equations.[11]

Equation (18) has no stability limitation on the size of the time step and hence offers the potential of great efficiency when compared to the explicit technique described above. The only practical limit on the time step size is due to accuracy; the larger the time step, the less accurate the transient solution will be.

Boundary Conditions

The boundary conditions are of five types: solid, inflow, outflow, centerline, and the farfield. These boundary types are illustrated in Fig. 3.

The no-slip condition is imposed at all solid boundaries. This is specified by

$$u = v = 0 \tag{21}$$

and

$$T = T_B \quad \text{(isothermal boundary)} \tag{22}$$

or

$$\left.\frac{\partial T}{\partial n}\right|_B = 0 \quad \text{(adiabatic boundary)} \tag{23}$$

The boundary conditions at the inflow boundary depend upon whether the flow is subsonic or supersonic at that boundary. If the flow is subsonic, three flow properties are specified (stagnation pressure, stagnation temperature, and flow angle) and a method of characteristics (MOC) formulation is employed to calculate the fourth flow property. For supersonic inflow, all four flow properties (u, v, ϵ, and ρ) are specified.

The boundary condition at the outflow boundary also depends upon the Mach number at that boundary. For subsonic outflow, the static pressure is enforced and the remaining three variables are calculated using a MOC formulation. When the outflow is supersonic, all of the flow information comes from upstream and, consequently, no boundary condition can be specified. In the latter situation, the flow properties are calculated from a MOC formulation using upstream quantities.

On the centerline, the axisymmetry of the flowfield is enforced. Namely,

$$v = 0 \tag{24}$$

$$\frac{\partial u}{\partial y} = \frac{\partial \epsilon}{\partial y} = \frac{\partial \rho}{\partial y} = 0 \tag{25}$$

At the farfield boundary, the flow is at freestream conditions (freestream static pressure and temperature and purely axial flow). Generally, one cannot afford to include enough mesh to extend this boundary far enough to achieve this condition. Hence, in most analyses, there will be flow across this boundary; i.e., it will be either an inflow or an outflow boundary depending upon the flow situation. A MOC formulation is used to account for the possible combinations.

Results

Four analyses are presented to illustrate the type of results one may obtain with this technique. The first of these models the flowfield through a de Laval nozzle; the second and third are calculations of the flowfield through typical turbofan nozzles, and the fourth presents a typical turbofan thrust reverser analysis.

The de Laval nozzle is a standard American Society of Mechanical Engineers (ASME) test nozzle. The geometry is shown in Fig. 4a. The sharp radius of curvature presents a computationally difficult problem. The analysis used 50 cells axially and 20 cells radially.

A test vs theory comparison is presented in Fig. 4b. The nozzle pressure ratio was 4.763. The time step size in the analysis was 1×10^9 times larger than the explicit time step size. Hence, Newton's method was used to obtain the results. The experimental data are due to Cuffel et al.[15] The analysis compares very favorably with the data.

The convergence history of the ASME analysis is shown in Fig. 5. The upper surface pressure distribution is presented

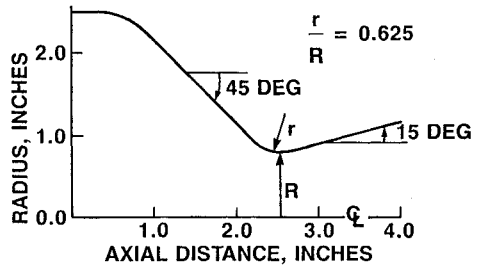

a) Geometry.

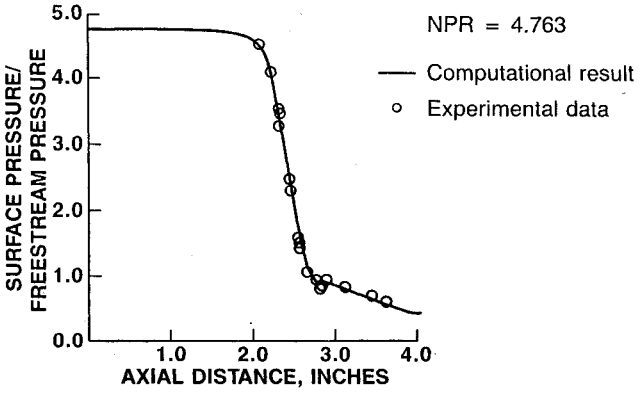

b) Surface pressures.

Fig. 4 ASME test nozzle.

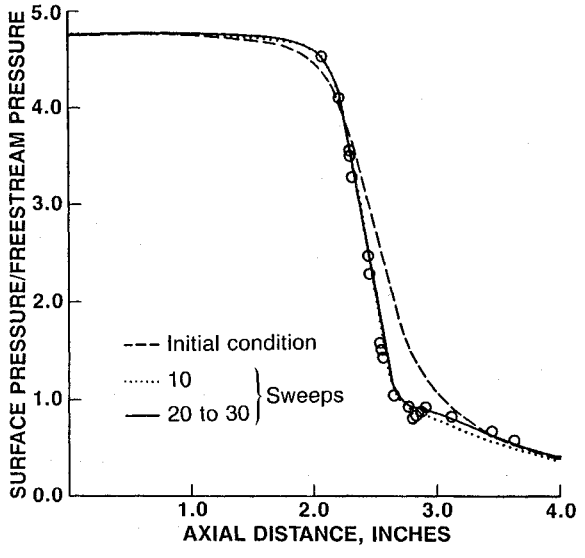

Fig. 5 ASME surface pressure convergence history.

every 10 sweeps for the first 30 sweeps. Examination of Fig. 5 reveals that the analysis converges after 20 sweeps.

The implicit technique required 1/40th the computer time necessary for the explicit method (16.7 vs 640.8 s, respectively, on the Cray X-MP computer).

The second case considered is also a test/theory comparison with data obtained from a scale model test of a fan and primary nozzle in the Boeing nozzle test facility. The geometry, called nozzle A, is shown in Fig. 6. The analysis used 88 cells axially and 35 cells radially. Two runs are presented. The first is subsonic, while the second models a transonic flow condition. In each case, the freestream condition was static (modeled herein with a Mach number of 0.1).

The subsonic analysis used the line Gauss-Seidel iteration technique with a time step size 1000 times larger than the allowable explicit time step. The solution converged in 70

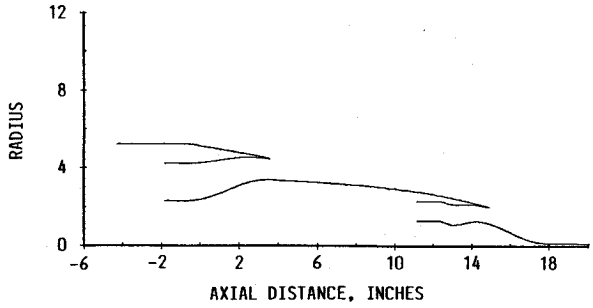

Fig. 6 Nozzle A geometry.

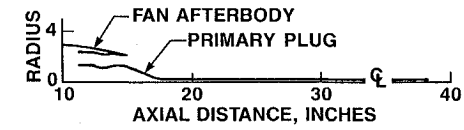

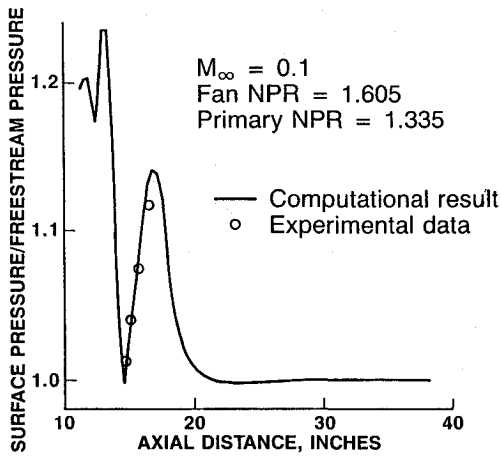

Fig. 7 Nozzle A subsonic analysis, primary plug pressure distribution.

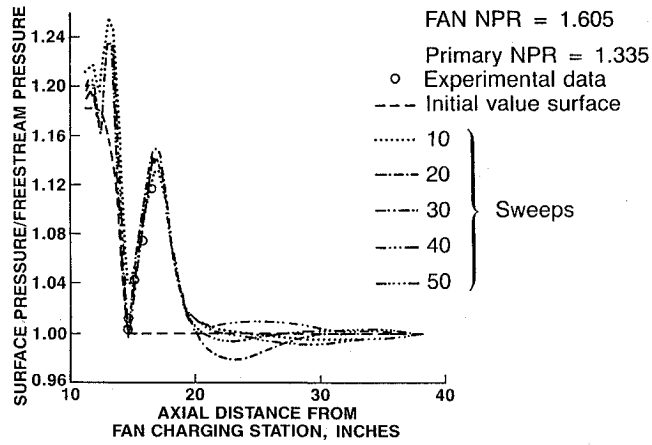

a) First 50 sweeps.

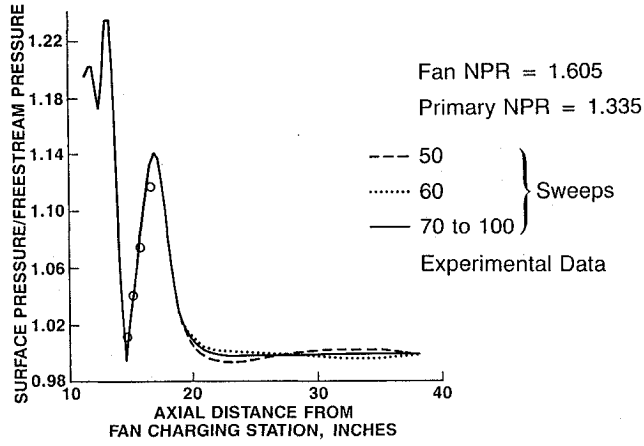

b) Second 50 sweeps.

Fig. 8 Nozzle A primary plug surface pressure convergence history.

iterations (151.6 CPU/s in the Cray X-MP computer; it is estimated that an explicit analysis would require 1500 s of computer time). The Baldwin-Lomax turbulence model was used.

Figure 7 illustrates the test/theory comparison of surface pressures along the primary plug for the subsonic analysis. The plug geometry is shown in Fig. 7a as an orientation for the flow results shown in Fig. 7b. Examination of that figure reveals an excellent comparison with data. Figure 8 shows the convergence history of the solution on the primary plug. Figure 8a illustrates the solution as it develops throughout the first 50 sweeps. It can be seen that the solution moves drastically from the initial value surface. Figure 8b gives the convergence history for the next 50 sweeps. The solution is converged after 70 sweeps.

Figure 9 presents the subsonic solution on the fan afterbody for nozzle A. The afterbody geometry is illustrated in Fig. 9a. The comparison with experiment (Fig. 9b) is quite good. The solution deviates near the cowl trailing edge because, having a finite thickness, it was modeled as a sharp point. Figure 10 depicts the convergence history on the fan afterbody for 50 sweeps. Examination of that figure reveals that the solution is converged after 30 sweeps.

The transonic analysis of nozzle A used the line Gauss-Seidel iteration technique with a variable time step size. The analysis started with the explicit time step size. The step size was increased by a factor of two raised to the one-eighth power each sweep. One hundred sweeps were taken. The progressive increase in time step size was necessary because of the shock waves on the fan afterbody and the primary plug. Because there are no shocks in the initial-value surface,

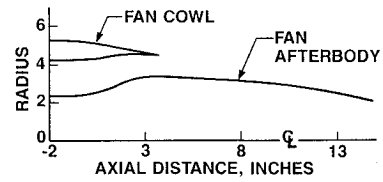

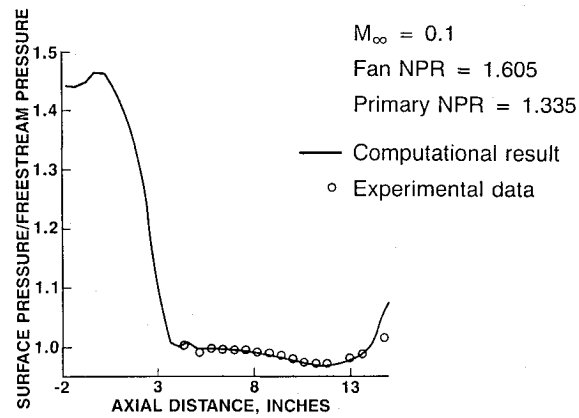

Fig. 9 Nozzle A subsonic analysis, fan afterbody pressure distribution.

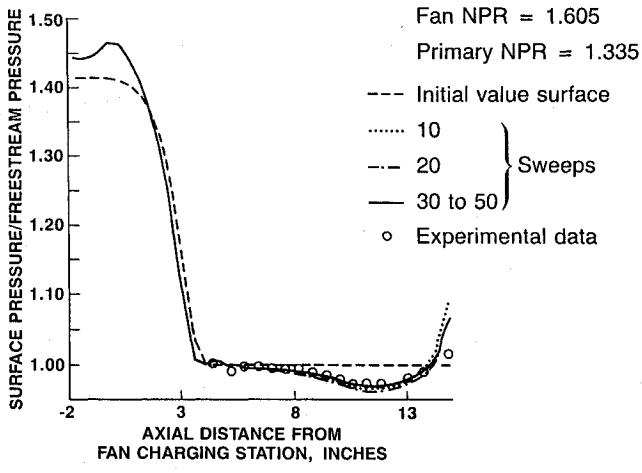

Fig. 10 Nozzle A, fan afterbody surface pressure convergence history.

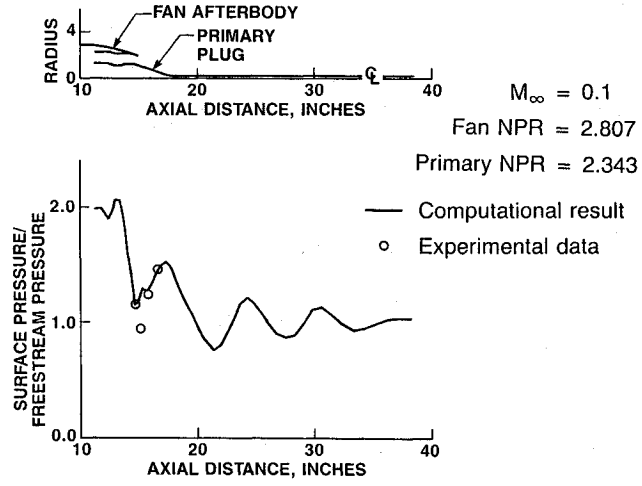

a) Primary plug.

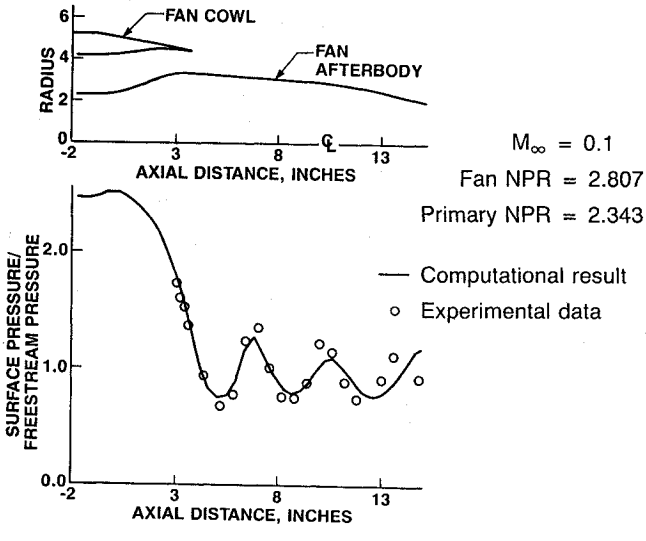

b) Fan afterbody.

Fig. 11 Nozzle A transonic analysis, pressure distribution.

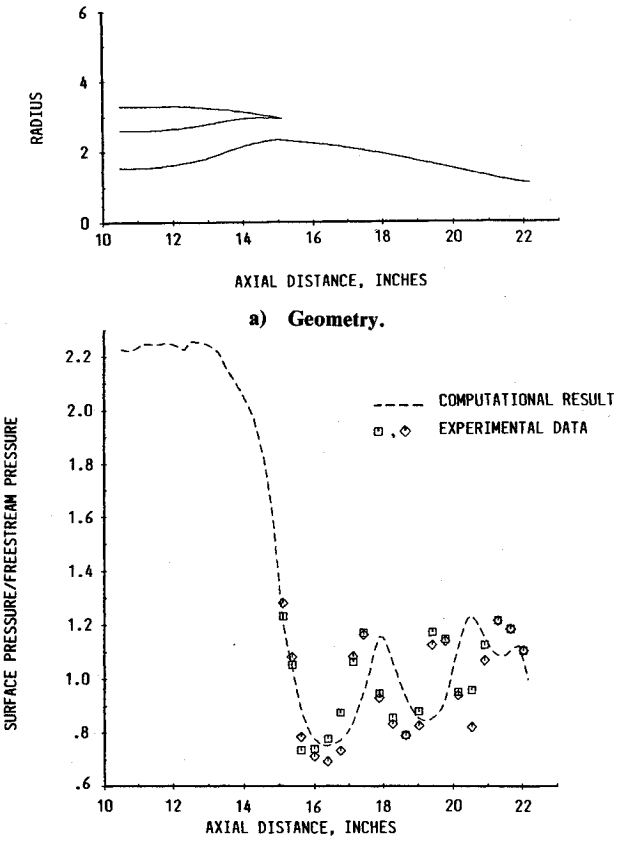

a) Geometry.

b) Calculated solution on fan afterbody.

Fig. 12 Nozzle B transonic analysis pressure distribution.

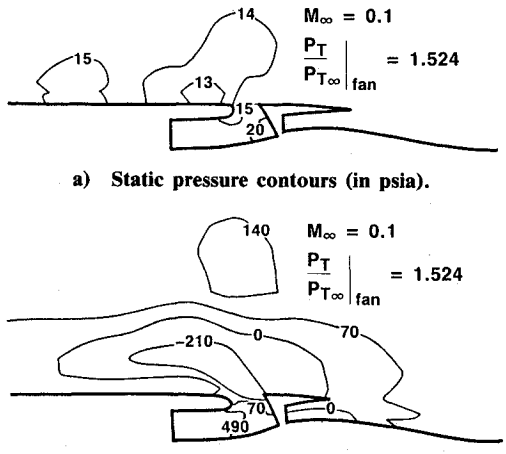

a) Static pressure contours (in psia).

b) Axial velocity contours (in ft/s).

Fig. 13 Typical turbofan thrust reverser analysis (positive velocities represent flow from left to right).

they have to develop as the calculation progresses. Hence, it is necessary initially to keep the time step size small; otherwise, the technique tends to move the shock too far each sweep, leading to instability.

Figure 11 presents the surface pressure distributions. Figure 11a illustrates the distribution of pressure along the primary plug and Fig. 11b the pressure distribution along the fan nozzle afterbody. The comparisons with experimental data are good. The discrepancies are due to lack of resolution in the mesh. The solution converged in 100 sweeps (236.5 s CPU time on the Cray X-MP computer).

The third case is an analysis of another turbofan nozzle, called nozzle B, at cruise. The freestream Mach number is 0.8 and the nozzle pressure ratio is 2.6. The line Gauss-Seidel iteration technique was used with the Baldwin-Lomax turbulence model. The same procedure for increasing the time step size that was used in the transonic analysis of nozzle A is used in this analysis. There are 96 cells axially and 96 cells radially. Figure 12a shows the geometry of nozzle B and Fig. 12b the calculated solution on the fan afterbody. The data are from a test in the Boeing 9×9 transonic wind tunnel. This analysis required 670 s on the Cray X-MP computer.

The fourth case is an analysis of a typical turbofan thrust reverser (axisymmetric representation). The results, shown in Fig. 13, were obtained using a time step size of five times larger than the explicit step size. The small value was used because an accurate transient solution was desired. Figure 13a shows the steady-state static pressure distribution (after 1000 sweeps). Figure 13b presents the steady-state distribution of the axial component of velocity. Three items of design interest can be determined from these results: 1) the load on the blocker door can be calculated; 2) the effective reverse thrust can be calculated by integrating the fluid property profiles; 3) during the transient solution, the static pressure at the fan nozzle decreased by 5 psi (due to an area mismatch in this design). This would represent an unacceptable engine mismatch that would be rectified in the final design. The thrust reverser analysis required 150 s on the Cray X-MP computer (55 axial cells by 30 radial cells).

Conclusions

Very good approximations to the solution of the Navier-Stokes equations are possible with this method. All of the numerical processes are second-order accurate. This means that halving the spatial step size will bring about a four-fold improvement in accuracy.

This computer program will give excellent predictions for the flowfields through axisymmetric, multistream geometries. If a solution for an extremely complex, but still axisymmetric, shape is desired, it could be obtained by adding enough mesh cells to resolve the features of the geometry adequately.

The line Gauss-Seidel implicit technique employed in this version of the code has given a two order of magnitude reduction in run time when compared to previous explicit technqiues.

The code requires 0.8 ms CPU time per mesh cell per sweep on the Cray X-MP computer. In general, the number of sweeps required for convergence is problem dependent. Experience has indicated that normal run requires 50–100 sweeps of convergence to steady state.

The Baldwin-Lomax algebraic mixing-length turbulence model, which is used in this analysis, yields an adequate representation of the physics of turbulence. The model has been used to analyze separated flow phenomena.[12] To date, however, this code has not been employed to predict separation.

The MacCormack line Gauss-Seidel implicit technique[11] represents a significant advancement in Navier-Stokes solution technology. Using this technique, an extension to three dimensions is feasible and, although the resulting code would be expensive to run, it would not be prohibitive. However, the development of a Navier-Stokes analysis tool that can be efficiently used in complex three-dimensional design studies will require further advancements in the solution algorithm area, as well as in geometry and mesh definition techniques.

Acknowledgments

The author would like to thank Professor Robert W. MacCormack of Stanford University who provided valuable assistance in the development and debugging of the code. The author would also like to thank Gary E. Shurtleff of Boeing Computer Services, who did some of the computer coding.

References

[1]Murman, E. M. and Cole, J. D., "Calculation of Plane Steady Transonic Flows," *AIAA Journal*, Vol. 9, Jan. 1971, pp. 114–121.

[2]Reyhner, T. A., "Three-Dimensional, Transonic Potential Flow About Complex Three-Dimensional Configurations," NASA CR-3814, July 1984.

[3]McLean, J. D. and Randall, J. L., "Computer Program to Calculate Three-Dimensional Boundary-Layer Flows over Wings with Mass Transfer," NASA CR-3123, 1978.

[4]Jameson, A., Schmidt, W., and Turkel, E., "Numerical Solutions of the Euler Equations by Finite Volume Methods Using Runge-Kutta Time-Stepping Schemes," AIAA Paper 81-1259, June 1981.

[5]Yu, N. J., Chen, H. C., Samant, S. S., and Rubbert, P. E., "Inviscid Drag Calculations for Transonic Flows," AIAA Paper 83-1928, July 1983.

[6]Perry, K. M. and Forester, C. K., "Numerical Simulation of Multi-Stream Nozzle Flows," *AIAA Journal*, Vol. 18, Sept. 1980, pp. 1088–1093.

[7]Cline, M. C. and Wilmoth, R. G., "Computation of High Reynolds Number Internal/External Flows," *AIAA Journal*, Vol. 21, Feb. 1983, pp. 171–173.

[8]MacCormack, R. W., "The Effect of Viscosity in Hypervelocity Impact Cratering," AIAA Paper 69-354, 1969.

[9]Beam, R. M. and Warming, R. F., "An Implicit Finite-Difference Algorithm for Hyperbolic Systems in Conservation Law Form," *Journal of Computational Physics*, Vol. 22, 1976, pp. 87–110.

[10]Pulliam, T. H., "Euler and Thin-Layer Navier-Stokes Codes: ARC2D, ARC3D," University of Tennessee Space Institute, Pub. E02-4005-023-84, 1984, p. 15.1.

[11]MacCormack, R. W., "Current Status of Numerical Solutions of the Navier-Stokes Equations," AIAA Paper 85-0032, Jan. 1985.

[12]Baldwin, B. S. and Lomax, H., "Thin Layer Approximations and Algebraic Model for Separated Turbulent Flows," AIAA Paper 78-257, 1978.

[13]Steger, J. and Warming, R. F., "Flux Vector Splitting of the Inviscid Gasdynamics Equations with Application to Finite Difference Methods," NASA TM-78605, 1979.

[14]Rusanov, V. V., "The Characteristics of General Equations of Gas Dynamics," *Zhurnal Vychislitel'noi Mathematicheskoi Fiziki*, Vol. 3, No. 3, 1963, pp. 508–527.

[15]Cuffel, R. F., Back, L. H., and Massier, P. F., "Transonic Flowfield in a Supersonic Nozzle with Small Throat Radius of Curvature," *AIAA Journal*, Vol. 7, July 1969, pp. 1364–1366.